Nuclear Physics B318 (1989) 301–318
North-Holland, Amsterdam

DEFLECTION OF GeV PARTICLE BEAMS BY CHANNELING IN BENT CRYSTAL PLANES OF CONSTANT CURVATURE

J S FORSTER, H HATTON and R J TOONE

Atomic Energy of Canada Limited Research Company, Chalk River Nuclear Laboratories, Chalk River, Ontario, Canada K0J 1J0

G ESTE

Advanced Technology Laboratory, Bell-Northern Research, P O Box 3511, Station C, Ottawa, Ontario, Canada K1Y 4H7

S I BAKER and R A CARRIGAN, JR

Fermi National Accelerator Laboratory, P O Box 500, Batavia, IL 60510, USA*

W M GIBSON and R L WIJAYAWARDANA**

Department of Physics, State University of New York at Albany, Albany, NY 12222, USA

J A ELLISON†

Department of Mathematics, University of New Mexico, Albuquerque, NM 87131, USA

L EMMAN-WORI

Department of Mathematics, New Mexico Institute of Mining and Technology, Socorro, NM 87131, USA

B O KOLBESEN

Zentrale Forschung and Entwicklung Forschunglaboratorien, Siemens AG, Postfach 832729, D-8000 Munchen 83, Fed Rep Germany

Received 3 October 1988

* Operated by Universities Research Association, Inc., under contract with the U S Department of Energy

** Now at Department of Physics, Faculty of Science, University of Peradeniya, Paradeniya, Sri Lanka

† This work was supported by the National Science Foundation under grants DMR-8214301 and DMR-8704348

The deflection of charged particle beams moving within the (110) planes of a 43 mm long silicon crystal has been observed for momenta from 60 to 200 GeV/c The crystal was bent by a 10 8 μm thick coating of ZnO along the central 26 mm of the crystal Measurements were made with the crystal at room temperature, where a total deflection of 32 5 mrad was observed, and with the crystal cooled to −145°C, where a 30 9 mrad deflection was observed The ratio of the number of particles that dechannel upon entering the bend to the number of initially channeled particles compares well with calculations based on the continuum model

1. Introduction

The deflection of a beam of charged particles moving within the planes of a bent crystal of silicon was first observed at Dubna with 8.4 GeV protons [1] Subsequently, a CERN–Aarhus–Strasbourg collaboration [2, 3] demonstrated both axial and planar bending at 12 GeV/c. In more recent experiments at Fermilab [4–6], the intensity loss of channeled particles along the crystal bend was studied for particle momenta between 12 and 180 GeV/c. The success of these experiments has resulted in the application of such crystal septa to replace bending magnets at 200 GeV/c [7] and at 800 GeV/c [8].

In all of these experiments, the crystal was bent by a three- or four-pin mechanical bending device In refs. [4, 5] it was shown, for a three-point bender, that a peak in the middle of the angular distribution of emergent particles occurred because of local distortions in the crystal produced by the center pin of the bending device. The use of a four-point bending device revealed two peaks in the deflected particle angular distribution corresponding to local distortions caused by the center two bending pins. However, for a given angle of deflection, the overall efficiency of the four-point bender considerably exceeds that of the three-point bender. This occurs because for a fixed deflection angle and a fixed distance between outer pins the maximum curvature in the four-point bender is less than the maximum curvature in the three-point bender. Although some theoretical work has been done on these variable curvature cases with a "slowly varying curvature assumption" [6], the most complete work to date is on the constant curvature case [9, 10]. Ideally, one would like a crystal which is bent in such a way as to produce constant curvature without the use of mechanical pins

We have produced a crystal with constant curvature by coating a Si slab with a thin layer (≈ 10 μm) of ZnO; the residual stresses caused by the ZnO result in a convex, uniform, circular bend on the side to which the ZnO is applied This crystal allows comparison with detailed calculations such as those of Ellison [9], Kudo [10], and Taratin and Vorobiev [11]. These calculations assume a uniform (i.e. constant radius of curvature) bend, and with this assumption earlier comparisons between experiment [5] and theory [9] proved difficult because of the variable curvature and the distortion caused by the pins in the bending device.

In this work, we report results for the deflection of charged particle beams of protons and pions from 60 to 200 GeV/c through a bending angle of > 30 mrad in

a constant curvature crystal. Data were collected for the bent silicon crystal operating at room temperature and at $\approx -145°C$ In sect. 2 we give experimental details; sect. 3 presents results and analysis and sect. 4 gives a comparison of the results with calculations based on Ellison [9] A summary and conclusions are given in sect. 5.

2. Experiment

The experiment was carried out in the M-Bottom beam of the Meson Laboratory at Fermilab. A plan view of the experimental layout is shown schematically in fig 1. The beam enters from the left through scintillator SC1 and drift chamber DC1. To reduce multiple scattering, the beam continues through a vacuum pipe ≈ 18.5 m long and then passes through drift chamber DC2 and scintillator SC2. It then enters the chamber containing the crystal and passes on through a tube, ≈ 10 m long, filled with helium gas at atmospheric pressure to reduce multiple scattering which would otherwise occur in air. Finally, the beam passes through drift chamber DC3 and scintillator SC3. Each drift chamber measures the beam particle's position event-by-event, in both x and y directions.

The middle scintillator, SC2, has a rectangular hole 1 mm wide by 5 mm high cut in the middle of it and acts as an anti-coincidence scintillator to ensure that only particles centered on the beam axis are counted. Fast timing signals are taken from

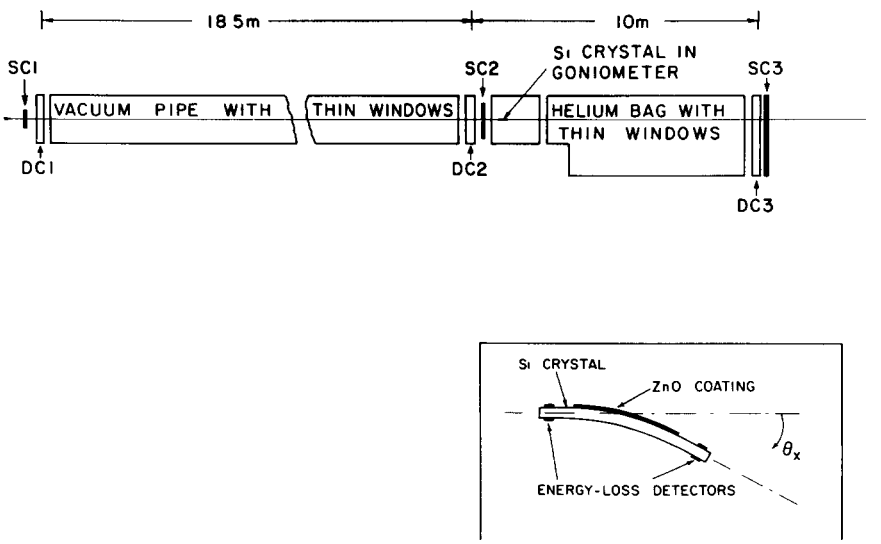

Fig 1 Plan view of the experimental apparatus The inset shows details of the ZnO coated crystal used in the experiment

the three scintillators and from the detector on the upstream end of the crystal and the coincidence requirement that SC1, SC3 and the crystal have fired, but not SC2, is made. If this is satisfied, then the energy-loss signals from the crystal and the timing information from the drift chambers are written onto magnetic tape.

The crystal is mounted in a three-axis goniometer which can be remotely stepped in angles θ_x, θ_y or ϕ. The rotation angle, ϕ, has steps of 0.01° which is adequate for positioning the crystal in the beam. The crystal is aligned for planar or axial channeling by movement in θ_x or θ_y and, because of the extremely small critical angles involved, the step size in these two angles is 0.0005°.

The crystal used in the present experiment was a slab 43 mm long by 11 mm high and 0.72 mm thick. It was cut from 50 kΩ cm, n-type silicon with a (110) plane parallel to the 43 mm by 11 mm face to better than 0.1° as determined by backscattered X-ray analysis and channeling measurements with a 1.0 MeV ^{4}He beam. An energy-loss detector was fabricated on each end of the crystal by implanting $\approx 10^{15}/\text{cm}^2$ B on one side of the slab and $\approx 10^{15}/\text{cm}^2$ P directly opposite over an area 3 mm along the slab by 8 mm high. One of the detectors was very noisy at room temperature but operated well when the crystal was cooled. The crystal was oriented to place this detector on the downstream end during the experiment so that the less noisy detector was used to select channeled particles based on lower energy loss.

To make a permanent bend on the crystal, ZnO was sputter coated onto one side of the slab over a 26 mm length centered on the crystal face. The ZnO coating was 10.8 μm thick, which resulted in ≈ 30 mrad total bend angle.

The crystal was mounted in the goniometer with the long face parallel to the beam and with the 12 mm side vertical i.e. the (110) plane vertical and parallel to the beam. Alignment of the (110) plane was achieved by moving the crystal in small increments in θ_x and observing the energy-loss spectrum from the detector on the upstream end of the crystal. Fig. 2 shows energy-loss spectra for an 80 GeV/c incident beam, when the crystal is aligned (a) and for random incidence (b). The critical angle at this momentum for (110) planar channeling of protons in Si is 17 μrad. Consequently, about 10% of the beam is within the critical angle and this is shown by the low-energy Landau peak in fig. 2.

Once the crystal was aligned, beam deflection measurements were made for 60, 80, 100, 120, 150, and 200 GeV/c momenta with the crystal at room temperature. The crystal was clamped lightly between the upstream detector and the ZnO coating. The detector holder was connected, via a copper braid, to a liquid nitrogen cold trap. An aluminum shroud, open at both ends in the beam direction, was mounted on the crystal holder to give radiative cooling as well as the direct cooling provided by the clamp. A thermocouple was mounted on the holder at the end furthest from the braid and, when the trap was filled with liquid nitrogen, recorded a temperature of −145°C. With the crystal cooled, measurements were again made for the same momenta as at room temperature.

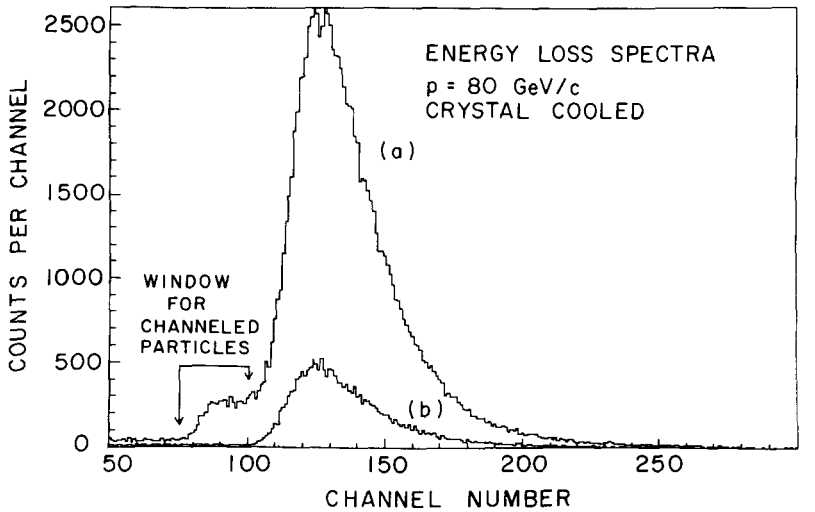

Fig 2 Energy-loss spectra for the Si crystal when (a) the (110) plane is aligned with the beam direction and (b) for random incidence, for 80 GeV/c with the crystal cooled

For each measurement approximately 100,000 events were recorded. For the 80 GeV/c measurement with the crystal cooled, an additional 300,000 events were collected to give data with lower statistical uncertainty in the region between the unbent and fully bent peaks in the angular distribution of emergent particles. Also, at 80 GeV/c with the crystal cooled, approximately 100,000 events were recorded with the crystal rotated ≈ 1 mrad in θ_x away from the aligned position, to obtain data for random incidence (cf. fig. 2).

3. Results and analysis

The event-by-event data were analyzed on the Concurrent Corporation 3230 minicomputer at Chalk River. To reconstruct the particle trajectories, event by event, the TDC's on all the drift chamber wires were calibrated with the beam by requiring a fast coincidence between SC1 and SC3 (see fig. 1); in this way we determined the time delay caused by the cables from the experimental area to the data collection area. With the known drift velocity, each particle's coordinates in x and y in the drift chambers, can then be determined. To calculate trajectories, the relative positions of the three drift chambers must be known. We chose to define the center of the undeflected beam in each drift chamber as the "zero" position.

During analysis at each momentum and crystal temperature, a window was set on the low energy portion of the energy-loss spectrum (see fig. 2) and the emergent angular distribution of particles determined. A two-dimensional intensity plot of the

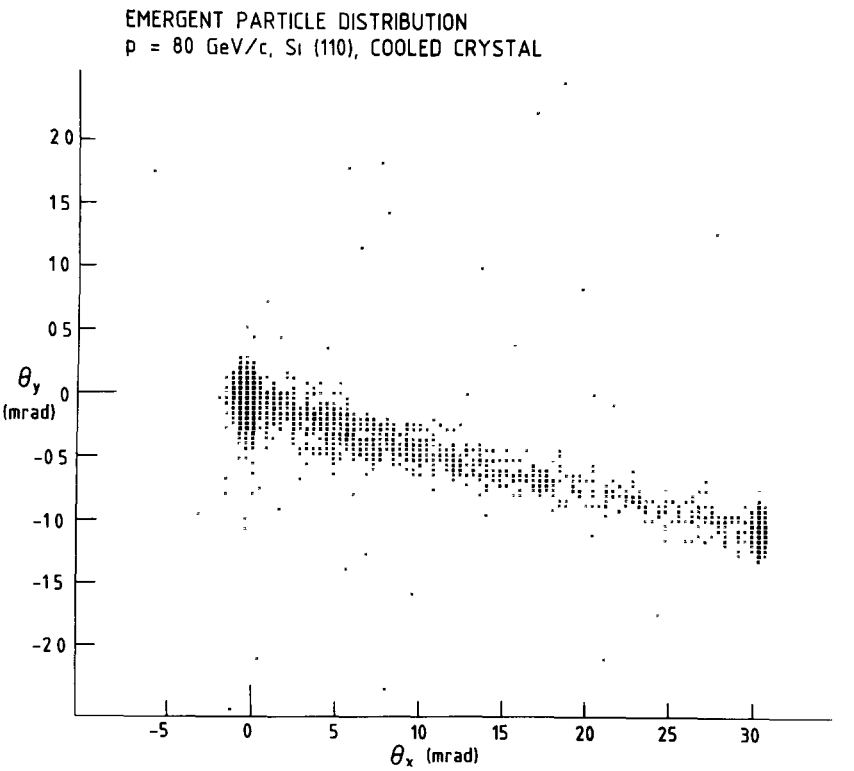

Fig 3 The emergent particle distribution for particles which are channeled at the front end of the crystal Note the different scales for θ_x and θ_y

outgoing angular distribution, θ_x vs. θ_y, for the 80 GeV/c cooled crystal data is shown in fig. 3. It can be seen that the darkest regions in the plot (highest intensity) occur (a) at $\theta_x \approx 0$ mrad corresponding to undeflected particles that dechannel because of multiple scattering between the energy-loss detector and the beginning of the bend, and that dechannel because of the bend, and (b) at $\theta_x \approx 30$ mrad corresponding to fully deflected particles. Most of the intensity is contained in these two regions with fewer particles in between that dechannel in the bend region. A projection of the data onto the θ_x direction (henceforward referred to as $\theta_{x_{out}}$) results in the spectra shown in figs. 4 and 5. Intensity vs. θ_x is shown for 60, 100, 150, and 200 GeV/c with the crystal at room temperatures (fig. 4) and with the crystal cooled (fig. 5). These figures show clearly the two separated peaks corresponding to undeflected and fully deflected particles. It is obvious that, for a given radius of curvature of the crystal, the number of particles that are fully deflected decreases as the momentum increases because of the higher centrifugal force experienced at the higher momenta.

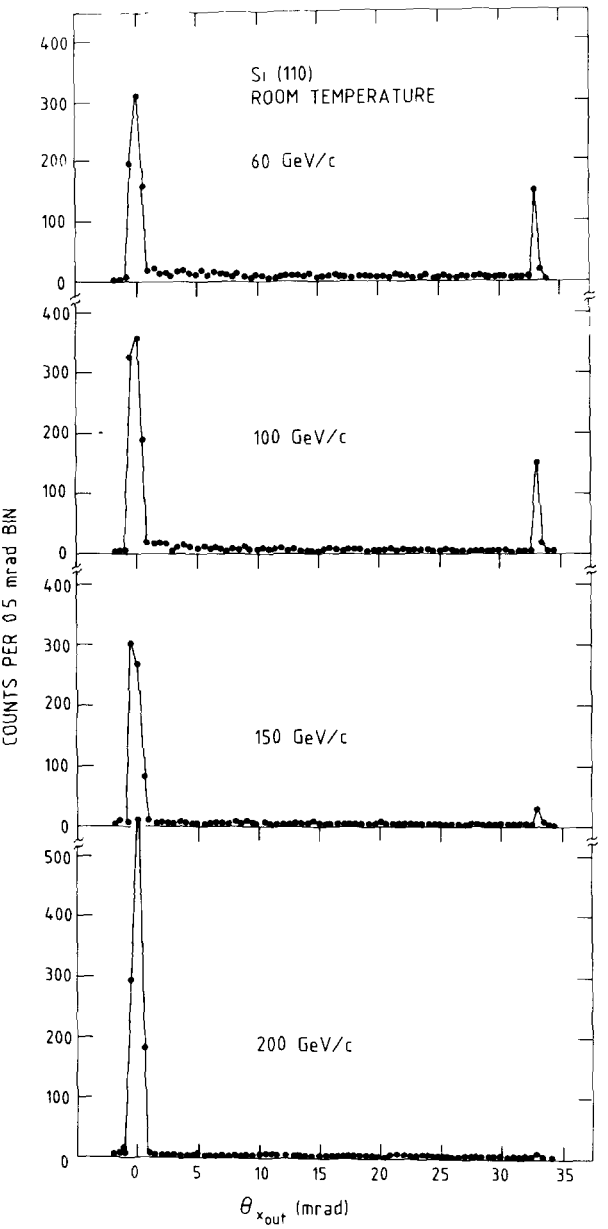

Fig 4 Emergent particle distributions in the bend direction of the crystal for momenta of 60, 100, 150 and 200 GeV/c with the crystal at room temperature

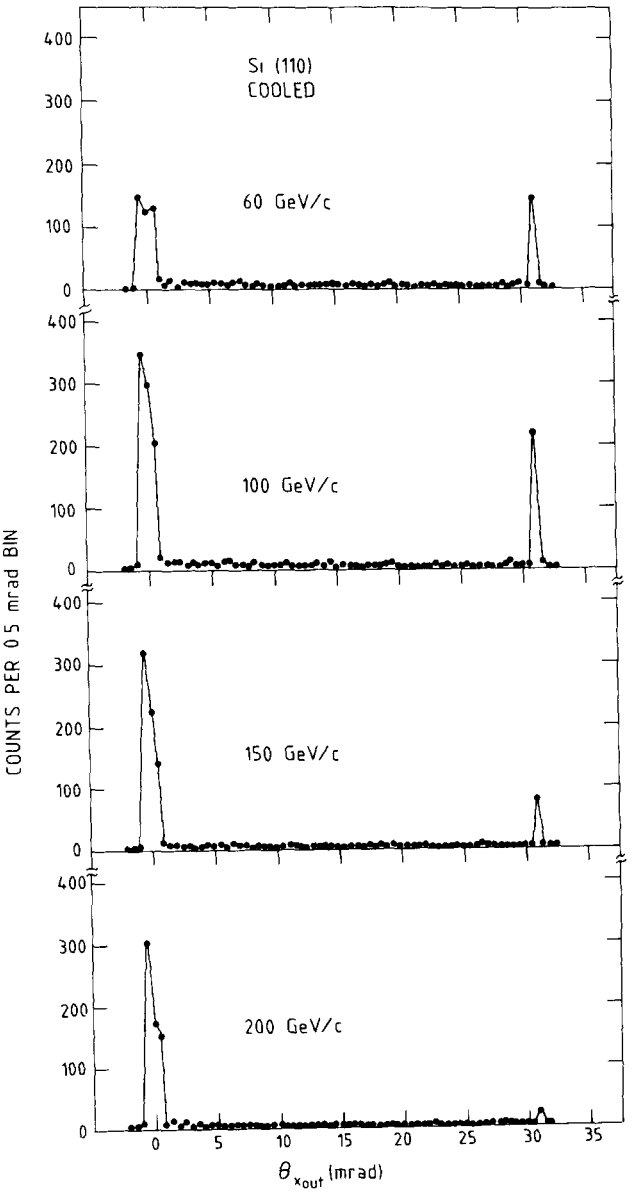

Fig 5 Same as for fig 4 but with the crystal cooled to $\approx -145°C$

3 1 MULTIPLE SCATTERING DECHANNELING IN THE BENT REGION

The distribution of particles between the undeflected and fully deflected regions shows little structure as would be expected for uniform curvature of the crystal In Ellison's model [9] all particles that are lost because of bending, dechannel within a short distance after entering the bend region. Therefore, the particles that appear between ≈ 2 mrad and ≈ 30 mrad in figs. 4 and 5 result from multiple scattering dechanneling. To investigate this dechanneling, we plot the number of channeled particles $I(\theta)$ versus θ where $I(\theta) = \int_{\theta}^{\infty} Y(\theta)\,\mathrm{d}\theta$ and $Y(\theta)$ is the number of counts per 0.5 mrad bin. Results for 150 GeV/c are shown in fig. 6 both for the crystal cooled and at room temperature and the data show an exponential dependence on angle. Since the curvature is constant in the bent region of the crystal, it is straightforward to convert the angle, θ, to distance, z, along the crystal length by

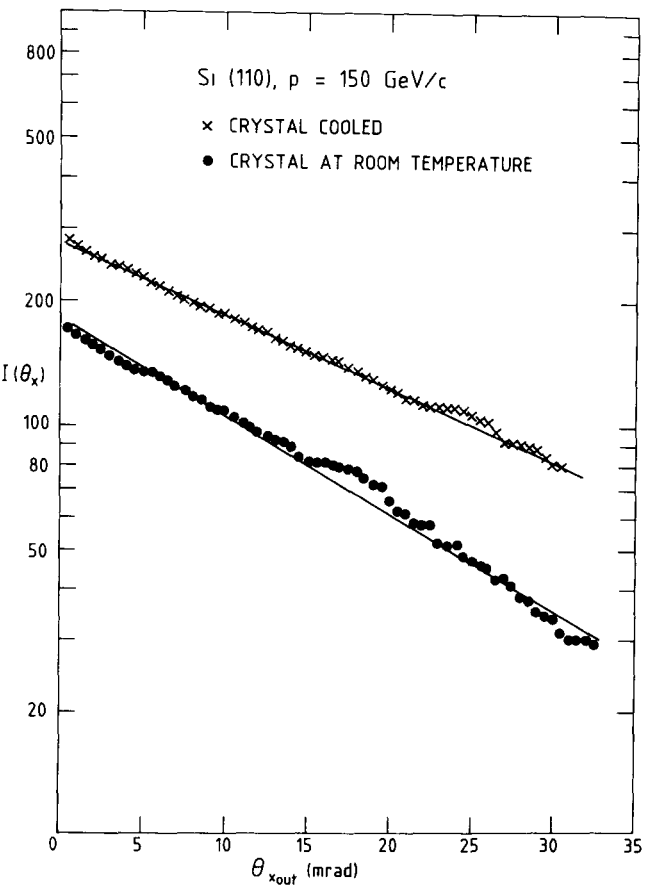

Fig 6 The number of particles channeled as a function of bend angle See text for details

TABLE 1
Dechanneling lengths for GeV/c protons and pions in the (110) plane of the bent Si crystal

p[GeV/c]	l_d [mm] (room temp)	l_d [mm] (cooled)
60	19 9 ± 0 4	22 6 ± 0 6
80	22 3 ± 0 6	28 8 ± 0 4
100	22 6 ± 0 6	27 8 ± 0 7
120	20 4 ± 0 6	26 9 ± 0 8
150	14 7 ± 0 4	20 8 ± 0 6
200	10 5 ± 0 4	18 1 ± 0 8

$\theta = z/R$ where R is the radius of curvature. By fitting an exponential function to the data, it is possible to extract a dechanneling length, l_d (the $1/e$ value). Results for our twelve sets of data are summarized in table 1 and are shown in fig. 7 where we have plotted the dechanneling length versus beam momentum, p; the uncertainties are statistical only. All of the data points for the cooled crystal lie above the room temperature data as one would expect because of the lower thermal vibrational amplitude of the Si atoms brought about by the cooling. From table 1, it can

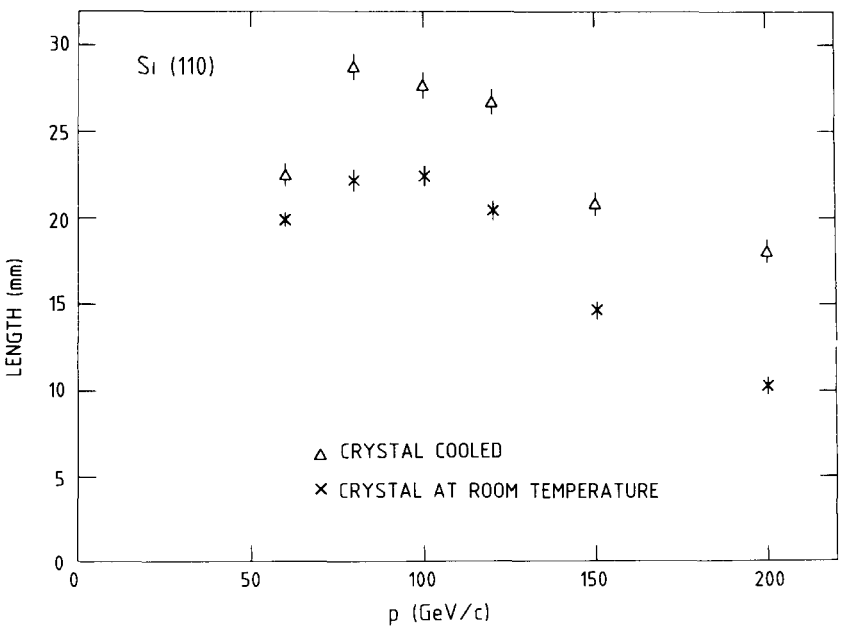

Fig 7 Dechanneling lengths, as a function of momentum, in the bent Si crystal

be seen that the dechanneling length increases by $\approx 14\%$ at 60 GeV/c to $\approx 70\%$ at 200 GeV/c by cooling the crystal.

Also, in fig. 7, we observe that, for a given temperature, the dechanneling length increases with beam momentum and then decreases This contrasts with a straight crystal in which the dechanneling length increases roughly linearly with beam energy or momentum. The reason for this is as follows. In the constant curvature case, the channeled particles oscillate about an equilibrium position, x_e, which is displaced by the centrifugal force from midway between the planes (as in an unbent crystal); x_e increases with increasing momentum going from zero, midway between the planes, to $dp/2$. Thus for x_e small, the dechanneling length should be approximately the straight crystal value. However, as x_e increases, the effective critical angle decreases (see fig 1 of ref. [9]) and the channeled particles interact with a larger electron density. Each of these causes a decrease in the slope of l_d vs. p, eventually causing l_d to decrease with increasing p. Thus we expect l_d as a function of x_e to reach a maximum and then decrease as x_e approaches $dp/2$. This behaviour is shown in fig. 8 where it is seen that the dechanneling length begins to decrease at $x_e/(dp/2) \approx 0.3$. Electron multiple scattering calculations with a diffusion equation approach are in progress [12] in order to quantify this momentum dependence and compare with the present experimental data.

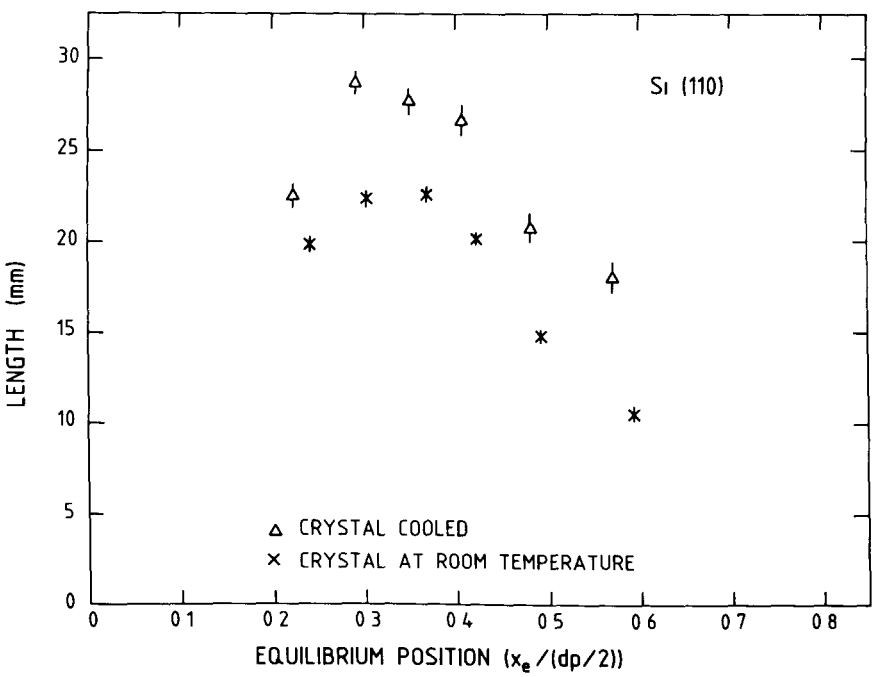

Fig 8 Dechanneling lengths, as a function of the equilibrium position, $x_e/(dp/2)$, in the bent Si crystal

3 2 EFFECTS OF ZnO COATING

In the earlier experiments [1–5] with mechanical bending devices, the silicon crystal was bent only in one direction (along the length of the crystal). In our case, using a ZnO coating to produce the bend, we do not only have bending along the length of the crystal, which gives the deflected beam, but also bending perpendicular

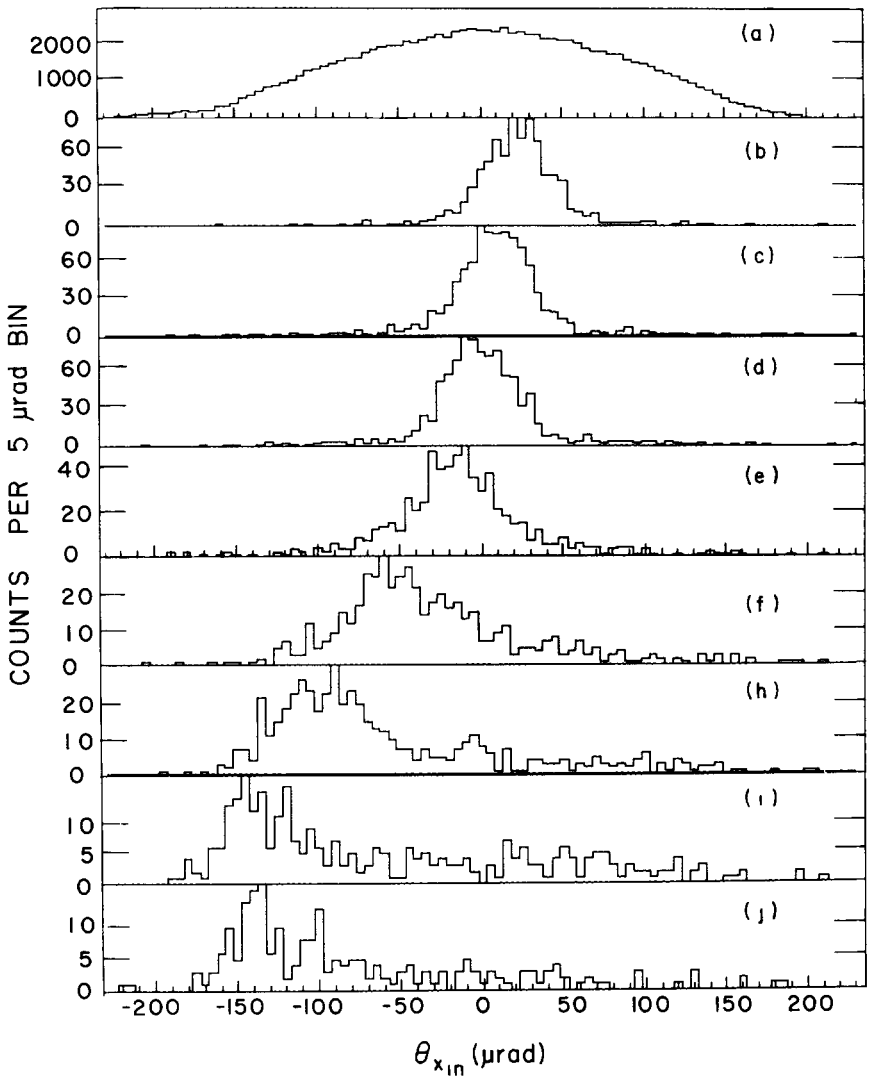

Fig. 9 Incoming angular distributions, $\theta_{x_{in}}$, as a function of vertical position in the crystal for the 80 GeV/c cooled crystal data (a) Beam envelope, (b–e) for 0 5 mm wide windows on vertical position, (f–i) for 0 75 mm wide windows on vertical position, (b) corresponds to the top of crystal and (i) to the bottom

to the beam direction. Over the vertical 12 mm face of the crystal, assuming the same Young's modules in both x and y-directions, we expect a total bending of $\simeq 13.9$ mrad. However, as pointed out in sect. 2, the anti-coincidence scintillator, SC2, selects the center 5 mm of the crystal which would give a maximum bending in the y-direction of $\simeq 5.8$ mrad. The result of such bending is shown in fig. 9 where we show the angular distribution of particles entering the crystal as a function of vertical position on the crystal. Fig. 9a shows the envelope of beam particles incident on the crystal in the x direction i.e across the (110) plane Figs 9b–9i show the same incident angular distribution but for a window set on low energy-loss particles (cf. fig. 2) and as a function of vertical position; fig. 9b corresponds to the top of the crystal while fig. 9i corresponds to the bottom

It is evident that the ZnO coating causes a distortion of the crystal resulting in the observed position of the (110) plane changing by ≈ 200 μrad from top to bottom. This is considerably less than 5.8 mrad estimated above and is probably a result of the channeled particles being defined by the energy-loss detector which is centered 5 mm upstream of the beginning of the ZnO coating. The width of each distribution however, is approximately 35–40 μrad FWHM as expected since $2\psi_p = 34$ μrad for 80 GeV/c particles in the Si (110) plane.

The other result of the ZnO coating is reflected in the outgoing angular distribution of particles. In figs. 4 and 5, the data were plotted in 0.5 mrad bins. However, with higher resolution, we find structure in the distributions as shown in fig. 10. Fig.

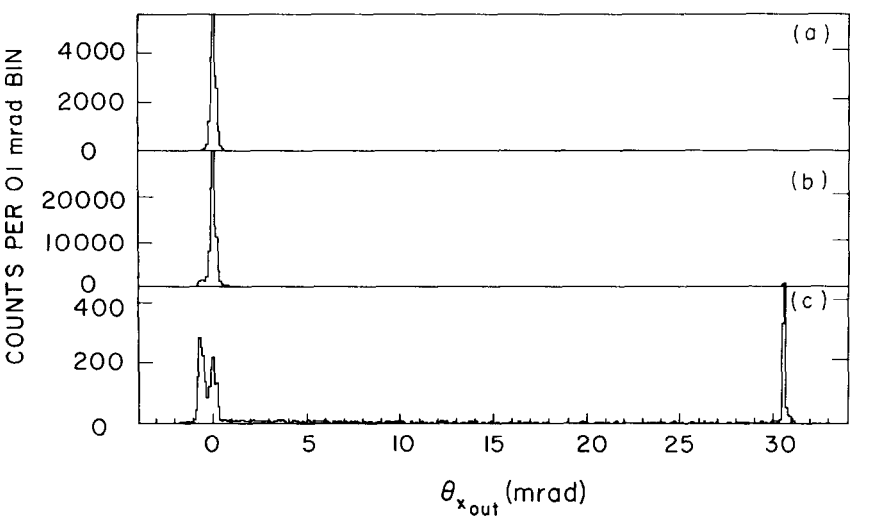

Fig 10 Outgoing angular distributions, $\theta_{x_{out}}$, in the bend direction for the 80 GeV/c cooled crystal data (a) Random incidence of beam, (b) (110) plane aligned with beam, (c) same as (b) but for a window on low energy-loss (channeled) particles

10a is the outgoing angular distribution in the x-direction (bend direction) for random incidence. Fig. 10b is the corresponding case for the crystal aligned and fig. 10c is the same as fig. 10b but for a window on low energy-loss. Both figs. 10b and 10c show a peak to the left of the main beam indicating a deflection in the direction opposite to the bend direction! This second peak is obviously a result of steering by the crystal since it disappears when the crystal is rotated ≈ 1 mrad from alignment of the (110) plane, as shown in fig. 10a.

We have investigated this effect by looking at the region about the beam direction, centered on 0 mrad in fig. 10, by setting a window on low energy-loss i.e. channeled particles, and looking at the outgoing angular distribution of particles in the x-direction for windows on the position of the incident beam on the entrance end of the crystal. Three windows in x (0.25 mm wide) and four windows in y (1.25 mm wide) were set on the crystal, as seen by the beam, and the resulting outgoing angular distributions in the x-direction are shown in fig. 11. The results for the incoming particles (fig. 9) showed an effect in going vertically along the crystal but the outgoing distributions show a left–right asymmetry. Most of the initially channeled particles which dechannel in the left side of the crystal result in the peak to the left of the main beam i.e. figs. 11a, d, g and j while those that dechannel in the right side of the crystal result in the peak centered on the beam direction. This effect occurred at all beam momenta and at both crystal temperatures.

We have no explanation for this except that it appears to be associated with the ZnO coating The deviation from a straight line due to the bending caused by the 26 mm long ZnO coating is 0.4 mm. This means that channeled particles entering the crystal on the left hand 0.4 mm of the 0 72 mm thick crystal, which become

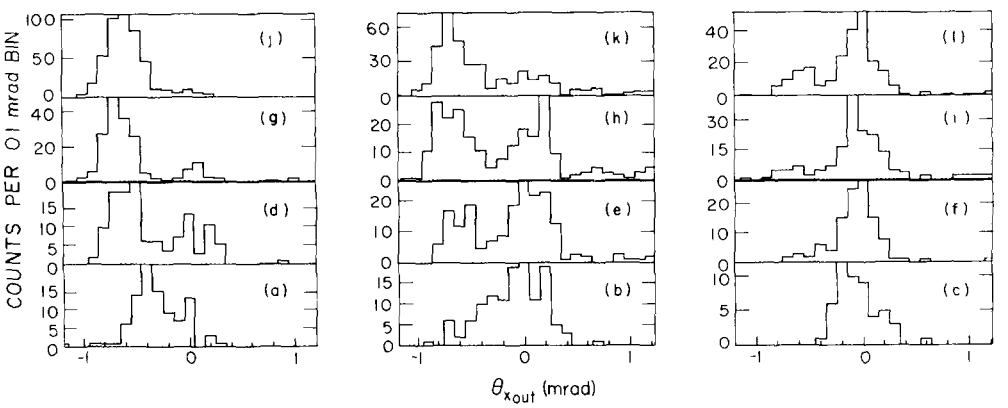

Fig 11 Outgoing angular distributions, $\theta_{x_{out}}$, about the beam direction for low-energy loss particles and as a function of the position of particles incident on the crystal for the 80 GeV/c cooled crystal data Fig (a) corresponds to lower left, (j) to upper left, (c) to lower right and (l) to upper right See text for details

dechanneled, exit through the ZnO coating while those particles on the remaining 0.32 mm which dechannel do not encounter ZnO; this assumes dechanneling to be a gradual increase in transverse energy such that the angle to the plane becomes a few times the critical angle, i.e. no violent collisions. This picture is consistent with what is observed in fig. 11.

We note that these effects on the incoming and outgoing distributions, caused by the ZnO coating should have no effect on the analysis described in the next section.

4. Comparison with calculations

The inset in fig. 1 shows a schematic of the beam and crystal. The beam enters the crystal at the left end and a channeled beam is selected at the energy-loss detector. This channeled beam moves through the straight portion with some dechanneling due to multiple scattering, enters the bend which causes bending dechanneling as discussed in ref. [9], moves through the constant curvature region with further dechanneling due to multiple scattering, enters the straight region with no bending dechanneling and continues in the downstream straight portion with the usual multiple scattering dechanneling. The particles that are dechanneled leave the crystal at roughly the angle at which they were dechanneled. The particles channeled all the way through the crystal exit at the full crystal deflection angle. This picture ignores feeding-in [13]. In ref. [9], a framework for calculating the dechanneled fraction, F, due to bending, as a function of $pv\kappa$, where $\kappa = 1/R$ is the constant curvature, was presented. The main assumptions used are that (1) the channeled particles are in statistical equilibrium when they reach the bend, (2) a particle dechannels if it penetrates too close to a plane, (3) the particle wavelength in the bend is shorter than the length of the bend, and (4) the bent planes can be modeled with a planar continuum potential. As a consequence of (2) and (3), bending dechanneling takes place in the first wavelength of particle motion after the particles enter the bend. In the present experiment, the incident beam has a large angular spread with respect to the channeling critical angle. Hence, the incident channeled beam is roughly uniformly distributed in both angle and space Since a uniform distribution in phase space is a statistical equilibrium distribution, we assume, consistent with ref. [9], that the distribution upon entering the bend is uniform in phase space. Thus the dechanneled fraction is simply $F = (A_0 - A_t)/A_0$ where A_0 is the phase space area of the channeled particles just before entering the bend and A_t is the phase space area of the particles which remain channeled after the onset of the bend (see fig. 1, ref [9]). In fig. 12, the values of F are plotted versus the dimensionless parameter, Γ, defined as

$$\Gamma = pv\kappa/2\pi Z_1 Z_2 e^2 n\,, \tag{1}$$

where p is the beam momentum, v is the beam velocity, κ is the curvature, Z_1 and

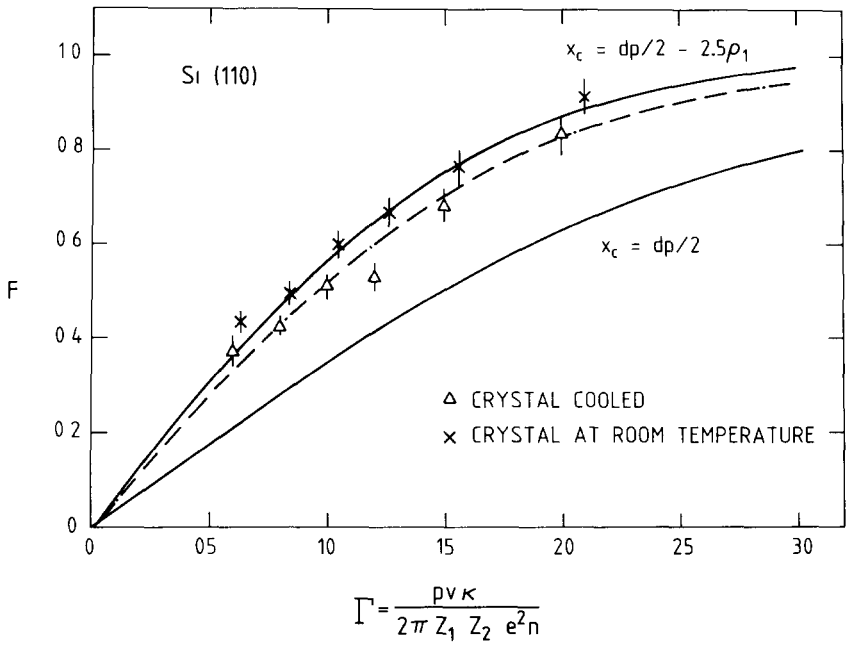

Fig 12 The dechanneled fraction, F, as a function of the dimensionless momentum parameter, Γ, for the room temperature and cooled crystal data

Z_2 are the atomic number of the projectile and target, respectively, e is the electronic charge and n is the areal density of each plane. The results for the (110) planes of Si for dechanneling at 2.5 $\rho_1(T)$ from the planes for our two temperatures are shown; also shown is the result for dechanneling at the planes ($dp/2$). Here, $\rho_1(T)$ is the one-dimensional root mean square lattice vibrational amplitude, T is the temperature and $\rho_1 = 0.057$ Å and 0.075 Å for $T = 128$ K and 293 K, respectively. This dechanneling criterion was chosen as a consequence of a recent study [14] of scattering from crystal planes where the authors find a rapid transition from conservation to non-conservation of transverse energy at an impact parameter of $\approx 2.5\rho_1$

From the data in figs. 4 and 5, it is possible to extract the dechanneled fraction due to bending for comparison with fig. 12. If we let N_1 denote the total number of particles in the peak at 0 mrad, N_2 denote the number in the peak at 0 mrad due to multiple scattering dechanneling between the energy-loss detector and the bend and N denote the total number of particles, then the dechanneled fraction due to bending is $F = (N_1 - N_2)/(N - N_2)$. These values are given in table 2 and shown in fig. 12 for the room temperature case (crosses) and the cooled case (open triangles) where the uncertainties shown are due to statistics only. N_2 has been calculated with results from a separate experiment [13]. The uncorrected F values ($F = N_1/N$) are

TABLE 2
Measured dechanneled fraction, F, as a function of momentum

p (GeV/c)	F (room temp)	F (cooled)
60	0 432 ± 0 027 (0 506)[a]	0 372 ± 0 031 (0 454)
80	0 494 ± 0 030 (0 563)	0 425 ± 0 015 (0 488)
100	0 600 ± 0 030 (0 636)	0 512 ± 0 026 (0 556)
120	0 670 ± 0 034 (0 696)	0 529 ± 0 030 (0 567)
150	0 766 ± 0 043 (0 780)	0 688 ± 0 037 (0 707)
200	0 919 ± 0 042 (0 923)	0 836 ± 0 048 (0 844)

[a] The numbers shown in parentheses are the F values before correction for multiple scattering dechanneling in the straight portion of the crystal between the energy-loss detector and the beginning of the bent region See text for details

shown in brackets and show the magnitude of the correction to F for multiple scattering dechanneling between the energy-loss detector and the beginning of the bent region. Since the data for dechanneling in a straight crystal [13] were only measured at room temperature, the correction to the data for the cooled crystal could be an overestimate, i.e. N_2 is larger than it should be which results in F being slightly smaller than it should be. However, low energy planar dechanneling experiments, for the (110) plane in Si, for 0.5 to 1.5 MeV protons [15] and for 3 0 MeV protons [16] show a temperature dependence of $\approx 10\%$ for the temperature range of this experiment. Therefore, the use of room temperature multiple scattering dechanneling data to correct the cooled crystal results should not be significant.

From fig. 12, it can be seen that there is good agreement between theory and experiment both for F vs. Γ and for the temperature dependence. In particular, it indicates that the dechanneling criterion of $2.5\rho_1$ is reasonable (it should be noted that $2.5\rho_1$, at room temperature, is approximately equal to the Thomas–Fermi screening distance, a_T).

5. Summary and conclusions

A silicon crystal coated with ZnO, has been used to deflect high-energy beams of protons and pions through angles as great as 32.5 mrad. The ZnO coating results in a region of constant curvature where the ZnO is applied, which makes it straightforward to compare the dechanneled fraction of initially channeled particles, as a function of momentum, with calculations based on the continuum model.

Measurements were made at room temperature, where a total deflection of 32.5 mrad was observed, and at -145°C, where a total deflection of 30.9 mrad was observed. The data agree very well with calculations based on dechanneling occurring at a distance of $2.5\rho_1$ from the planes.

Dechanneling lengths in the bent crystal were found to increase initially with increasing momentum and then decrease. The point at which the length begins to decrease occurs at an equilibrium position away from the center of the channel, $x_e/(dp/2)$, of 0.3.

Finally, we note that the ZnO coating causes a deflection of the dechanneled fraction of the beam in the opposite direction to that of the bend. The particles which are associated with this "negative angle" deflection are ones that are originally channeled but dechannel and exit through the ZnO coating.

The results obtained in this work make it possible to predict accurately the dechanneled fraction of initially channeled particles for a particular application. Since it is believed that the ZnO coating is of piezo-electric grade material, it may be possible to "fine tune" the deflection angle by a d.c. voltage applied between the uncoated side of the Si crystal and a metal electrode evaporated onto the ZnO.

We wish to thank I.V. Mitchell for his interest in this work and J.U Andersen for many stimulating discussions regarding planar dechanneling

References

[1] A F Elishev et al , Phys Lett B88 (1979) 387
[2] J F Bak et al , Phys Lett B93 (1980) 505
[3] J F Bak et al , Nucl Phys B242 (1984) 1
[4] S I Baker et al , Phys Lett B137 (1984) 129
[5] W M Gibson et al , Nucl Instr and Meth in Phys Res B2 (1984) 54
[6] J A Ellison et al , Nucl Instr and Meth in Phys Res B2 (1984) 9
[7] S I Baker et al , Nucl Instr and Meth in Phys Res A234 (1985) 602
[8] S I Baker et al , Nucl Instr and Meth in Phys Res A248 (1986) 301
[9] J A Ellison, Nucl Phys B206 (1982) 205
[10] H Kudo, Nucl Instr and Meth 189 (1981) 609
[11] A M Taratin and S A Vorobiev, Phys Status Solidi (b) 107 (1981) 521
[12] L Emman-Wori, Master's Thesis, New Mexico Institute of Mining and Technology, 1988
[13] J S Forster, *in* Relativistic channeling, NATO, ASI Series B Physics, Vol 165, ed R A Carrigan, Jr and J A Ellison, (Plenum, New York, 1987)
[14] J U Andersen, J Bak and E Bonderup, Nucl Instr and Meth in Phys Res B33 (1988) 34
[15] S U Campisano, G Foti, F Grasso, M Lo Savio and E Rimini, Radiat Eff 13 (1972) 157
[16] J A Davies, J Denhartog and J L Whitton, Phys Rev 165 (1968) 345